fluids

MDPI

Article

Heat and Mass Transfer Analysis on Magneto Micropolar Fluid Flow with Heat Absorption in Induced Magnetic Field

Md. Mohidul Haque

Mathematics Discipline, Science Engineering and Technology School, Khulna University, Khulna 9208, Bangladesh; mmhaque@math.ku.ac.bd

Abstract: Heat and mass transfer due to a magneto micropolar fluid flow along a semi-infinite vertical plate bounded by a porous medium are investigated in presence of induced magnetic field. In case of cooling flow, heat and mass fluxes from the plate are subjected to be constant under the action of a constant heat sink. Mathematical model related to the problem is developed from the basis of studying magnetohydrodynamics (MHD) for both lighter and heavier particles. Dimensionless model of momentum, microrotation, induction, energy and concentration equations are solved simultaneously by the explicit scheme of finite difference technique. According to the obtained stability and convergence criteria of this transient flow, very negligible time step ($\Delta t = 0.002$) compared to the existing works has been taken to perform the numerical computation. Quantities of chief physical interest of the flow as shear stress, couple stress, current density, Nusselt number and Sherwood number are also studied here. The numerically computed results are compared with published results of available research works. Interestingly an excellent agreement is found with finite difference solutions in both explicit and implicit schemes. In order to discuss the physical aspects of the problem, the flow variables for different values of associated parameters are illustrated in graphs. Finally, important findings of the study are listed as concluding remarks.

Keywords: MHD; heat and mass transfer; micropolar fluid; induced magnetic field; finite difference method; heat absorption

Citation: Haque, M.M. Heat and Mass Transfer Analysis on Magneto Micropolar Fluid Flow with Heat Absorption in Induced Magnetic Field. *Fluids* **2021**, *6*, 126. https://doi.org/10.3390/fluids6030126

Academic Editor: Ioannis Sarris

Received: 31 January 2021
Accepted: 15 March 2021
Published: 19 March 2021

1. Introduction

The behaviors of fluid that contain suspended, metal or dust particles in many practical situations are first observed by the micropolar fluid theory of Eringen [1] with internal structures in which coupling between the spin of each particle and the macroscopic velocity field is taken into account. Physically, the micropolar fluids contain dilute suspension of small, rigid, cylindrical macromolecules with individual motion and are influenced by spin inertia. The theory is used to investigate the flow character of polymeric fluids, colloidal suspension, human and animal blood, liquid crystal, exotic lubricants etc. Micropolar fluid dynamic has attracted the attention of a large number of scientists due to its diverse applications at the present time. The thermo-micropolar fluid theory of Eringen [2] is developed by extending the theory of micropolar fluid.

The free convective micropolar fluid flow induced by the simultaneous action of buoyancy forces is of great interest in nature and in many industrial applications as drying processes, solidification of binary alloy as well as in astrophysics, geophysics and oceanography. Jena and Mathur [3] have obtained a similarity solution for laminar free convective flow of thermo-micropolar fluid from a non-isothermal vertical flat plate. A numerical boundary layer solution for a steady free convective micropolar fluid flow from a vertical isothermal plate is computed by Gorla et al. [4].

Many engineering applications such as condensation, extraction, drying of solid materials, evaporation, rectification, distillation and absorption of fluids are affected by the

combined heat and mass transfer processes. A free convection with mass transfer flow for a micropolar fluid bounded by a vertical surface under the action of a transverse magnetic field is analyzed by El-Amin [5]. The unsteady free convective heat and mass transfer micropolar fluid flow through a vertical infinite porous medium under the action of a transverse magnetic field taking into account a constant heat source with constant heat and mass fluxes has been studied numerically by Haque et al. [6]. Effects of thermal radiation on micropolar fluid flow was observed by Bhattacharyya et al. [7]. Safaei et al. [8] analyzed a boundary layer heat transfer flow of water/FMWCNT (functionalized multi-walled carbon nanotube) nanofluids along a flat plate. Convective flows of different types of fluid due to stretching sheet/surface have been analyzed by the authors in the references [9–15]. Gaffar et al. [16] have developed a mathematical model to investigate the free convective flow in a third-grade viscoelastic micropolar fluid from a vertical isothermal inverted cone. Scholars in the references [17–21] have studied convective flows along plate embedded in a porous medium. Recently, Karvelas et al. [22] have used a micropolar fluid model to study the auto rotation effect of human blood's microstructure on its flow.

A strong magnetic field due to a force of the field radiating from the poles of the magnet induces a new magnetic field known as induced magnetic field which is applied in many astrophysical and geophysical problems. From the point of natural and industrial applications, several numbers of investigators have given a special attraction to observe the induced magnetic field effect on the flow problems. Concerning this, investigators in the references [23–25] analyzed the induced magnetic field effect on combined heat and mass transfer one/two dimensional flows. The micropolar fluid behavior on magnetohydrodynamics (MHD) heat transfer unsteady flow through an infinite porous plate with induced magnetic field has studied by Sultana et al. [26]. In a rotating system, a numerical simulation with stability analysis on MHD natural convective heat and mass transfer unsteady flow with induced magnetic field was finished by Haque et al. [27]. A MHD stagnation point flow of nanofluid with induced magnetic field is observed by Ibrahim [28]. The influence of magnetic field on blood flow has studied numerically by Hossain and Haque [29]. The micromagnetorotation (MMR) effect on a micropolar fluid flow is studied by Aslani et al. [30]. In order to control the cooling rate and achieve the desired quality of industrial products, researchers in the references [31–33] have investigated the flow characteristics in the presence of induced magnetic field under different environments.

Recently, Baruah and Hazarika [34] have investigated a heat and mass transfer unsteady flow of micripolar fluid over a stretching sheet under the action of a transverse magnetic field. The magnetic Reynolds number in the study was taken as small enough to neglect the induced magnetic field. The flow problem becomes more complicated when it is affected by an induced magnetic field, heat absorbing source, constant heat and mass fluxes as well as a vertical plate instead of stretching sheet. Hence the research efforts in the present work are devoted to study the effects of induced magnetic field on the transient heat and mass transfer magneto micropolar fluid flow past a semi-infinite vertical plate surrounded by a porous medium in the presence of a constant heat sink. These types of fluid flows have special importance in geophysical fluid dynamics and play a decisive role in a number of industrial applications.

2. Flow Model of the Physical Problem

A natural convective heat and mass transfer unsteady flow of an electrically conducting incompressible viscous micropolar fluid past an electrically non-conducting semi-infinite vertical plate embedded in a porous medium is considered here. The fluid flow is generated due to the gravitational acceleration and the pressure gradient along the normal direction of the plate. A strong magnetic field has also been applied near to the plate so that the plate becomes magnetized. An induced magnetism is produced by the force of the field radiating from the poles of the magnet. In this case, heat and mass transfer due to the micropolar fluid flow is affected by an induced magnetic field.

In geometrical concept, the Cartesian coordinate system is chosen in such way that the x-axis is measured along the plate in upward direction and y-axis is normal to the plate. The appropriate physical configuration of the flow with coordinate system is displayed in Figure 1.

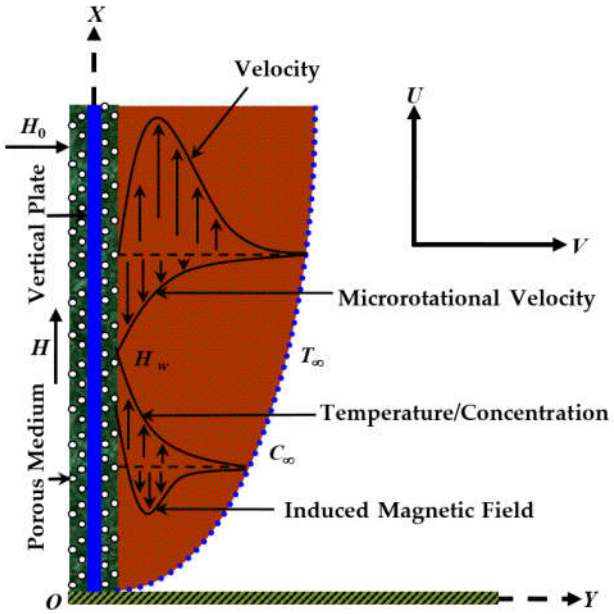

Figure 1. Physical Configuration with Coordinate System.

At the beginning of this research work, the system with magneto micropolar fluid is kept at uniform temperature (T_∞) and species concentration (C_∞). In addition, the analysis is based on the following assumptions:

i. All the physical properties of fluid are considered to be constant but the influence of density variation with temperature is assumed only in the body force term, in accordance with the well-known Boussinesq's approximation.
ii. Since the plate is of semi-infinite extent and the fluid motion is unsteady so all the flow variables will depend upon the distance variable along the plate x, distance variable normal to the plate y and the time variable τ.
iii. The microrotation vector of the form $\mathbf{G}=\left(0, 0, \bar{\Gamma}\right)$ is considered here.
iv. The viscous dissipation and joule heating terms in the energy equation have been assumed for high speed flow as well as a constant heat sink h_s is used for heat absorption [35].
v. The level of concentration of foreign mass has been taken very high for observing the thermal diffusion effect on flow. The mass diffusion effect has also been studied here.
vi. The magnetic Reynolds number is taken to be large enough so that the induced magnetic field vector of the form $\mathbf{H}=\left(H_x, H_y, 0\right)$ is applicable. The divergence equation of Maxwell's equation $\nabla.\mathbf{H}=0$ for the magnetic field gives $H_y =$ constant $= H_0$ (say).

Within the framework of the above stated assumptions, the equations relevant to the heat generating free convective heat and mass transfer unsteady flow of micropolar fluid with induced magnetic field are governed by the following system of coupled non-linear partial differential equations under the boundary-layer approximations,

Continuity Equation,

$$\frac{\partial u}{\partial x}+\frac{\partial u}{\partial y}=0$$

Momentum Equation,

$$\frac{\partial u}{\partial \tau}+u\frac{\partial u}{\partial x}+v\frac{\partial u}{\partial y}=g\beta\left(\overline{T}-T_{\infty}\right)+g\beta^{*}\left(\overline{C}-C_{\infty}\right)+\left(\upsilon+\frac{\chi}{\rho}\right)\frac{\partial^{2}u}{\partial y^{2}}+\frac{\chi}{\rho}\frac{\partial\overline{\Gamma}}{\partial y}-\frac{\upsilon}{K}u+\frac{\mu_{e}}{\rho}H_{0}\frac{\partial H_{x}}{\partial y}$$

Microrotation Equation,

$$\frac{\partial\overline{\Gamma}}{\partial \tau}+u\frac{\partial\overline{\Gamma}}{\partial x}+v\frac{\partial\overline{\Gamma}}{\partial y}=\frac{\gamma}{\rho j}\frac{\partial^{2}\overline{\Gamma}}{\partial y^{2}}-\frac{\chi}{\rho j}\left(2\overline{\Gamma}+\frac{\partial u}{\partial y}\right)$$

Magnetic Induction Equation,

$$\frac{\partial H_{x}}{\partial \tau}+u\frac{\partial H_{x}}{\partial x}+v\frac{\partial H_{x}}{\partial y}=H_{x}\frac{\partial u}{\partial x}+H_{0}\frac{\partial u}{\partial y}+\frac{1}{\sigma\mu_{e}}\frac{\partial^{2}H_{x}}{\partial y^{2}}$$

Energy Equation,

$$\frac{\partial\overline{T}}{\partial \tau}+u\frac{\partial\overline{T}}{\partial x}+v\frac{\partial\overline{T}}{\partial y}=\frac{\kappa}{\rho c_{p}}\frac{\partial^{2}\overline{T}}{\partial y^{2}}+\frac{1}{\rho c_{p}\sigma}\left(\frac{\partial H_{x}}{\partial y}\right)^{2}+\frac{1}{c_{p}}\left(\upsilon+\frac{\chi}{\rho}\right)\left(\frac{\partial u}{\partial y}\right)^{2}+\frac{D_{m}\kappa_{T}}{c_{s}c_{p}}\frac{\partial^{2}\overline{C}}{\partial y^{2}}-\frac{h_{s}}{\rho c_{p}}\left(\overline{T}-T_{\infty}\right)$$

Concentration Equation,

$$\frac{\partial\overline{C}}{\partial \tau}+u\frac{\partial\overline{C}}{\partial x}+v\frac{\partial\overline{C}}{\partial y}=D_{m}\frac{\partial^{2}\overline{C}}{\partial y^{2}}+\frac{D_{m}\kappa_{T}}{T_{m}}\frac{\partial^{2}\overline{T}}{\partial y^{2}}$$

Since the heat and mass fluxes from the plate to fluid through porous medium are constant, hence the initial conditions becomes,

$$\tau\le 0,\quad u=0,\quad v=0,\quad \overline{\Gamma}=0,\qquad H_{x}=0,\quad \overline{T}\to T_{\infty},\qquad \overline{C}\to C_{\infty}\qquad \text{everywhere}$$

and the appropriate boundary conditions are as follows,

$$\tau>0,\quad u=0,\quad v=0,\quad \overline{\Gamma}=0,\qquad H_{x}=0,\quad \overline{T}\to T_{\infty},\qquad \overline{C}\to C_{\infty}\qquad \text{at } x=0$$

$$u=0,\quad v=0,\quad \overline{\Gamma}=\frac{-S\partial u}{\partial y},\quad H_{x}=H_{w},\quad \frac{\partial\overline{T}}{\partial y}=\frac{-Q}{\kappa},\quad \frac{\partial\overline{C}}{\partial y}=\frac{-m}{D_{m}}\qquad \text{at } y=0$$

$$u=0,\quad v=0,\quad \overline{\Gamma}=0,\qquad H_{x}=0,\quad \overline{T}\to T_{\infty},\quad \overline{C}\to C_{\infty}\qquad \text{as } y\to\infty$$

3. Mathematical Formulation

Mathematical model of the magneto micropolar fluid flow is a system of coupled non-linear partial differential equations. To solve this flow problem, the model must be dimensionless. Hence the following non-dimensional quantities have been taken to make the governing equations dimensionless;

$$X=\frac{xU_{0}}{\upsilon},\ Y=\frac{yU_{0}}{\upsilon},\ U=\frac{u}{U_{0}},\ V=\frac{v}{U_{0}},\ t=\frac{\tau U_{0}^{2}}{\upsilon},\ \Gamma=\frac{\overline{\Gamma}\,\upsilon}{U_{0}^{2}},\ H=\sqrt{\frac{\mu_{e}}{\rho}}\frac{H_{x}}{U_{0}},\ T=\frac{\kappa U_{0}\left(\overline{T}-T_{\infty}\right)}{Q\upsilon}\ \text{ and }\ C=\frac{D_{m}U_{0}\left(\overline{C}-C_{\infty}\right)}{m\upsilon}.$$

After simplification the following nonlinear coupled partial differential equations in terms of non-dimensional variables are obtained,

Dimensionless Continuity Equation,

$$\frac{\partial U}{\partial X}+\frac{\partial V}{\partial Y}=0$$

Dimensionless Momentum Equation,

$$\frac{\partial U}{\partial t}+U\frac{\partial U}{\partial X}+V\frac{\partial U}{\partial Y}=G_rT+G_mC+(1+\Delta)\frac{\partial^2 U}{\partial Y^2}+\Delta\frac{\partial \Gamma}{\partial Y}-D_aU+M\frac{\partial H}{\partial Y}$$

Dimensionless Microrotation Equation,

$$\frac{\partial \Gamma}{\partial t}+U\frac{\partial \Gamma}{\partial X}+V\frac{\partial \Gamma}{\partial Y}=\Lambda\frac{\partial^2 \Gamma}{\partial Y^2}-\lambda\left(2\Gamma+\frac{\partial U}{\partial Y}\right)$$

Dimensionless Magnetic Induction Equation,

$$\frac{\partial H}{\partial t}+U\frac{\partial H}{\partial X}+V\frac{\partial H}{\partial Y}=H\frac{\partial U}{\partial X}+M\frac{\partial U}{\partial Y}+\frac{1}{P_m}\frac{\partial^2 H}{\partial Y^2}$$

Dimensionless Energy Equation,

$$\frac{\partial T}{\partial t}+U\frac{\partial T}{\partial X}+V\frac{\partial T}{\partial Y}=\frac{1}{P_r}\frac{\partial^2 T}{\partial Y^2}+(1+\Delta)E_c\left(\frac{\partial U}{\partial Y}\right)^2+\frac{E_c}{P_m}\left(\frac{\partial H}{\partial Y}\right)^2+D_f\frac{\partial^2 C}{\partial Y^2}-\frac{\alpha}{P_r}T$$

Dimensionless Concentration Equation,

$$\frac{\partial C}{\partial t}+U\frac{\partial C}{\partial X}+V\frac{\partial C}{\partial Y}=\frac{1}{S_c}\frac{\partial^2 C}{\partial Y^2}+S_o\frac{\partial^2 T}{\partial Y^2}$$

and the corresponding initial and boundary conditions become,

$t\le 0,\quad U=0,\quad V=0,\quad \Gamma=0,\quad H=0,\quad T=0,\quad C=0$ everywhere

$t>0,\quad U=0,\quad V=0,\quad \Gamma=0,\quad H=0,\quad T=0,\quad C=0$ at $X=0$

$$U=0,\quad V=0,\quad \Gamma=-S\frac{\partial U}{\partial Y},\quad H=h=1(\text{say}),\quad \frac{\partial T}{\partial Y}=-1,\quad \frac{\partial C}{\partial Y}=-1 \text{ at } Y=0$$

$$U=0,\quad V=0,\quad \Gamma=0,\quad H=0,\quad T=0,\quad C=0 \quad \text{as } Y\to\infty$$

where, $h=\frac{H_w}{U_0}\sqrt{\frac{\mu_e}{\rho}}=1(\text{say}),\quad G_r=\frac{g\beta Q\upsilon^2}{\kappa U_0^4},\quad G_m=\frac{g\beta^* m\upsilon^2}{D_m U_0^4},\quad \Delta=\frac{\chi}{\upsilon\rho},\quad D_a=\frac{\upsilon^2}{U_0^2 K},$

$\Lambda=\frac{\gamma}{\upsilon j\rho},\quad \lambda=\frac{\chi\upsilon}{\upsilon j U_0^2},\quad M=\frac{H_0}{U_0}\sqrt{\frac{\mu_e}{\rho}},\quad P_m=\upsilon\sigma\mu_e,\quad P_r=\frac{\upsilon\rho c_p}{\kappa},\quad E_c=\frac{\kappa U_0^3}{Q\upsilon c_p},\quad \alpha=\frac{h_s\upsilon^2}{\kappa U_0^2},$

$S_c=\frac{\upsilon}{D_m},\quad S_o=\frac{Q D_m^2\kappa_T}{m\kappa\upsilon T_m}$ and $D_f=\frac{\kappa m\kappa_T}{Q\upsilon c_s c_p}$.

The quantities of chief physical interest of the flow near at the plate such as the skin friction coefficients, current density, heat transfer rate and mass transfer rate are also studied here. In order to obtain the numerical values of those quantities, it is arbitrarily chosen that the length of the semi-infinitely extended plate is $X_{\max}(=100)$ and the length of the boundary layer thickness is $Y_{\max}(=25)$ as corresponding to $Y\to\infty$ which lies very well outside the boundary layers. Hence the flow region within the boundary layer is found as a rectangle with sides $X_{\max}$ and $Y_{\max}$.

One of the skin friction coefficients is shear stress so the local and average shear stress at the plate $(Y=0)$ are proportional to $\left(\frac{\partial U}{\partial Y}\right)_{Y=0}$ and $\int_0^{100}\left(\frac{\partial U}{\partial Y}\right)_{Y=0}dX$ respectively. Another skin friction coefficients is couple stress whose local and average part are proportional to $\left(\frac{\partial \Gamma}{\partial Y}\right)_{Y=0}$ and $\int_0^{100}\left(\frac{\partial \Gamma}{\partial Y}\right)_{Y=0}dX$ respectively. The local and average current density at the plate are proportional to $\left(-\frac{\partial H}{\partial Y}\right)_{Y=0}$ and $\int_0^{100}\left(-\frac{\partial H}{\partial Y}\right)_{Y=0}dX$ respectively. The

local and average Nusselt number are proportional to $\left(-\frac{\partial T}{\partial Y}\right)_{Y=0}$ and $\int_0^{100}\left(-\frac{\partial T}{\partial Y}\right)_{Y=0} dX$ respectively. Last of all, the local and average Sherwood number are proportional to $\left(-\frac{\partial C}{\partial Y}\right)_{Y=0}$ and $\int_0^{100}\left(-\frac{\partial C}{\partial Y}\right)_{Y=0} dX$ respectively.

4. Numerical Computation

Due to the complexity of finding an analytical solution of the system of second order nonlinear coupled partial differential equations, a numerical technique must be applied to solve this problem. For simplicity, an explicit procedure of finite difference method is used to obtain a numerical solution. In order to formulate a system of finite difference equations, the rectangular region of flow within the boundary layer is divided into a grid or mesh of lines parallel and normal to the plate. After carrying out the trial with a different number of grid lines, 100 grid lines are fixed here. Hence the X-directional height of plate is divided by $m\,(=100)$ horizontal grid lines and the Y-directional thickness of boundary layer is divided by $n\,(=100)$ vertical grid lines. Therefore, the appropriate mesh sizes for computation become $\Delta X = 1.0$ and $\Delta Y = 0.25$ with a smaller time-step Δt = 0.002. The finite difference grid space is drawn in Figure 2.

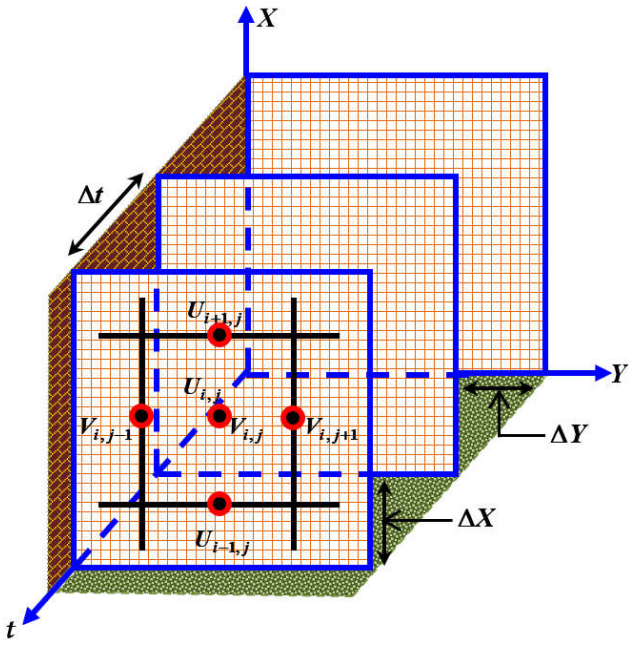

Figure 2. Finite Difference Grid Space.

Let U', V', Γ', H', T' and C' denote the values of U, V, Γ, H, T and C at the end of a time-step respectively. The following applicable set of finite difference equations is obtained using the explicit finite difference approximations,

Finite Difference Continuity Equation, $\frac{U'_{i,j} - U'_{i-1,j}}{\Delta X} + \frac{V_{i,j} - V_{i,j-1}}{\Delta Y} = 0$

Finite Difference Momentum Equation,

$$\frac{U'_{i,j} - U_{i,j}}{\Delta t} + U_{i,j}\frac{U_{i,j} - U_{i-1,j}}{\Delta X} + V_{i,j}\frac{U_{i,j+1} - U_{i,j}}{\Delta Y} = G_r T'_{i,j} + G_m C'_{i,j} - D_a U'_{i,j}$$

$$+\left(1+\Delta\right)\frac{U_{i,j+1}-2U_{i,j}+U_{i,j-1}}{\left(\Delta Y\right)^2}+\Delta\frac{\Gamma_{i,j+1}-\Gamma_{i,j}}{\Delta Y}+M\frac{H_{i,j+1}-H_{i,j}}{\Delta Y}$$

Finite Difference Microrotation Equation,

$$\frac{\Gamma'_{i,j}-\Gamma_{i,j}}{\Delta t}+U_{i,j}\frac{\Gamma_{i,j}-\Gamma_{i-1,j}}{\Delta X}+V_{i,j}\frac{\Gamma_{i,j+1}-\Gamma_{i,j}}{\Delta Y}=\Lambda\frac{\Gamma_{i,j+1}-2\Gamma_{i,j}+\Gamma_{i,j-1}}{\left(\Delta Y\right)^2}-\lambda\left(2\Gamma'_{i,j}+\frac{U_{i,j+1}-U_{i,j}}{\Delta Y}\right)$$

Finite Difference Magnetic Induction Equation,

$$\frac{H'_{i,j}-H_{i,j}}{\Delta t}+U_{i,j}\frac{H_{i,j}-H_{i-1,j}}{\Delta X}+V_{i,j}\frac{H_{i,j+1}-H_{i,j}}{\Delta Y}=H_{i,j}\frac{U_{i,j}-U_{i-1,j}}{\Delta X}+M\frac{U_{i,j+1}-U_{i,j}}{\Delta Y}$$

$$+\frac{1}{P_m}\frac{H_{i,j+1}-2H_{i,j}+H_{i,j-1}}{\left(\Delta Y\right)^2}$$

Finite Difference Energy Equation,

$$\frac{T'_{i,j}-T_{i,j}}{\Delta t}+U_{i,j}\frac{T_{i,j}-T_{i-1,j}}{\Delta X}+V_{i,j}\frac{T_{i,j+1}-T_{i,j}}{\Delta Y}=\frac{1}{P_r}\frac{T_{i,j+1}-2T_{i,j}+T_{i,j-1}}{\left(\Delta Y\right)^2}-\frac{\alpha}{P_r}T'_{i,j}+\frac{E_c}{P_m}\left(\frac{H_{i,j+1}-H_{i,j}}{\Delta Y}\right)^2$$

$$+\left(1+\Delta\right)E_c\left(\frac{U_{i,j+1}-U_{i,j}}{\Delta Y}\right)^2+D_f\frac{C_{i,j+1}-2C_{i,j}+C_{i,j-1}}{\left(\Delta Y\right)^2}$$

Finite Difference Concentration Equation,

$$\frac{C'_{i,j}-C_{i,j}}{\Delta t}+U_{i,j}\frac{C_{i,j}-C_{i-1,j}}{\Delta X}+V_{i,j}\frac{C_{i,j+1}-C_{i,j}}{\Delta Y}=\frac{1}{S_c}\frac{C_{i,j+1}-2C_{i,j}+C_{i,j-1}}{\left(\Delta Y\right)^2}+S_o\frac{T_{i,j+1}-2T_{i,j}+T_{i,j-1}}{\left(\Delta Y\right)^2}.$$

The initial and boundary conditions based on the finite difference scheme are as follows,

$$U^0_{i,j}=0,\quad V^0_{i,j}=0,\quad \Gamma^0_{i,j}=0,\quad H^0_{i,j}=0,\quad T^0_{i,j}=0,\quad C^0_{i,j}=0$$

$$U^n_{0,j}=0,\quad V^n_{0,j}=0,\quad \Gamma^n_{0,j}=0,\quad H^n_{0,j}=0,\quad T^n_{0,j}=0,\quad C^n_{0,j}=0$$

$$U^n_{i,0}=0,\quad V^n_{i,0}=0,\quad \Gamma^n_{i,0}=-S\frac{U_{i,1}-U_{i,0}}{\Delta Y},\quad H^n_{i,0}=1,\quad T^n_{i,0}=T^n_{i,1}+\Delta Y,\quad C^n_{i,0}=C^n_{i,1}+\Delta Y$$

$$U^n_{i,L}=0,\quad V^n_{i,L}=0,\quad \Gamma^n_{i,L}=0,\quad H^n_{i,L}=0,\quad T^n_{i,L}=0,\quad C^n_{i,L}=0\qquad \text{where } L\to\infty$$

Here the subscripts i and j denote X and Y directional grid points respectively and the superscript n represents a value of time, $t=n\Delta t$ where $n=0, 1, 2,....$ From the initial condition, the values of U, Γ, H, T and C are known at $t=0$. At the end of any time-step Δt, the new temperature T', new concentration C', new velocity U', new microrotational velocity Γ', new induced magnetic field H' and V' at all interior nodal points may be obtained by successive applications of finite difference energy, concentration, momentum, microrotation, magnetic induction and continuity equations respectively. This process is repeated in time and provided the time-step is sufficiently small, hence U, V, Γ, H, T and C should eventually converge to values which approximate the steady-state solutions of the model.

The numerical values of local shear stress, couple stress, current density, Nusselt number and Sherwood number are evaluated by Five-point approximation formula

[36,37] for the derivative and then the average shear stress, couple stress, current density, Nusselt number and Sherwood number are calculated by Simpson's $\frac{1}{3}$ integration formula [36,37].

Since an explicit procedure is used as a solving method, so the technique is required to establish a stability and convergence criteria of the problem. After simplification by using the general terms of Fourier expansion for the flow variables, we have obtained $U\frac{\Delta t}{\Delta X}+|V|\frac{\Delta t}{\Delta Y}+\frac{2}{P_r}\frac{\Delta t}{(\Delta Y)^2}+\frac{\alpha\,\Delta t}{2\,P_r}\le 1$ and $U\frac{\Delta t}{\Delta X}+|V|\frac{\Delta t}{\Delta Y}+\frac{2}{S_c}\frac{\Delta t}{(\Delta Y)^2}\le 1$ as the stability criteria of the explicit finite difference method. Using the constant mesh sizes $\Delta X=1.0$ and $\Delta Y=0.25$ with the smaller time step $\Delta t=0.002,$ we have also found $D_f<1,\ E_c<<1,$ $P_r\ge 0.0641$ and $S_c\ge 0.064$ as the convergence conditions of the present problem.

5. Discussion of the Results

To investigate the practical aspect of the problem, a finite difference solution is obtained by the use of an explicit procedure. The numerical values of velocity, microrotational velocity, induced magnetic field, temperature and concentration within the boundary layer are computed by assigning the different values of associated parameters with the help of a software development product Parallel Studio XE (American Multinational Corporation and Technology Company Intel Corporation, Santa Clara, CA, USA) as a computer programming language FORTRAN. In order to get the steady-state solutions, the computations have been carried out up to $t=20$. It is observed that the numerical values of flow variables show little changes after the time $t=10$. Hence the steady-state solutions have been obtained at the maximum time $t=20$. In this case the numerical data of all flow variables are collected hare at the time $t=2,\ 4$ and 20.

In this study, the Grashof number $(G_r=5.0,\ 6.0,\ 7.0)$ for heat transfer and the modified Grashof number $(G_m=2.0)$ for mass transfer are taken to be positive, the values $G_r>0$ with $G_m>0$ correspond to cooling to the plate. Practically the cooling problem is often encountered in engineering applications as the cooling of electronic components and nuclear reactors. Since the most important fluids are known as atmospheric air, salt water and water so the values of Prandtl number are preferred $P_r=0.71$ (for air), $P_r=1.0$ (for salt water) and $P_r=7.0$ (for water) with respect to the convergence conditions of the problem. It is also considered that the investigation is performed for both lighter particles as helium $(S_c=0.3)$, water vapour $(S_c=0.6)$ and heavier particle carbondioxide $(S_c=1.0)$. The values of other associated parameters are also chosen arbitrarily.

To verify the accuracy of the present results, two graphical comparisons with existing numerical solutions are presented in Figure 3. If we use viscous fluid instead of micropolar fluid and neglect the effects of induced magnetic field, constant heat source, viscous dissipation, joule heating, thermal diffusion, mass diffusion as well as the plate is not subjected to constant heat and mass fluxes then the current fluid flow is transformed into a simple boundary layer flow of Callahan and Marner [36]. If we apply a transverse magnetic field on the transformed simple flow then we get the MHD flow of Palani and Srikanth [37]. At the time $t=0.6$, the velocity curve for the buoyancy ratio parameter $N=\frac{G_m}{G_r}=2.0,\quad P_r=1.0,\quad S_c=0.7,\quad M=0.0,\quad \Delta=0.0,\quad D_a=0.0,\quad \Lambda=0.0,\quad \lambda=0.0,$ $P_m=0.0,\ E_c=0.0,\ \alpha=0.0,\ D_f=0.0,\ S_o=0.0$ is compared with the explicit finite difference solution of Callahan and Marner [36], which are displayed in Figure 3a. Another comparison of velocity profile at $t=0.26$ for the values of non-zero parameters $N=2.0,$

$P_r = 0.7$, $S_c = 0.5$, $M = 1.0$ with the implicit finite difference solution of Palani and Srikanth [37] is shown in Figure 3b. It is found that the numerical results of present study are in excellent agreement with the results of previously available works in both schemes of finite difference method. Hence the accuracy of the current results may be described as very good in case of all the flow variables.

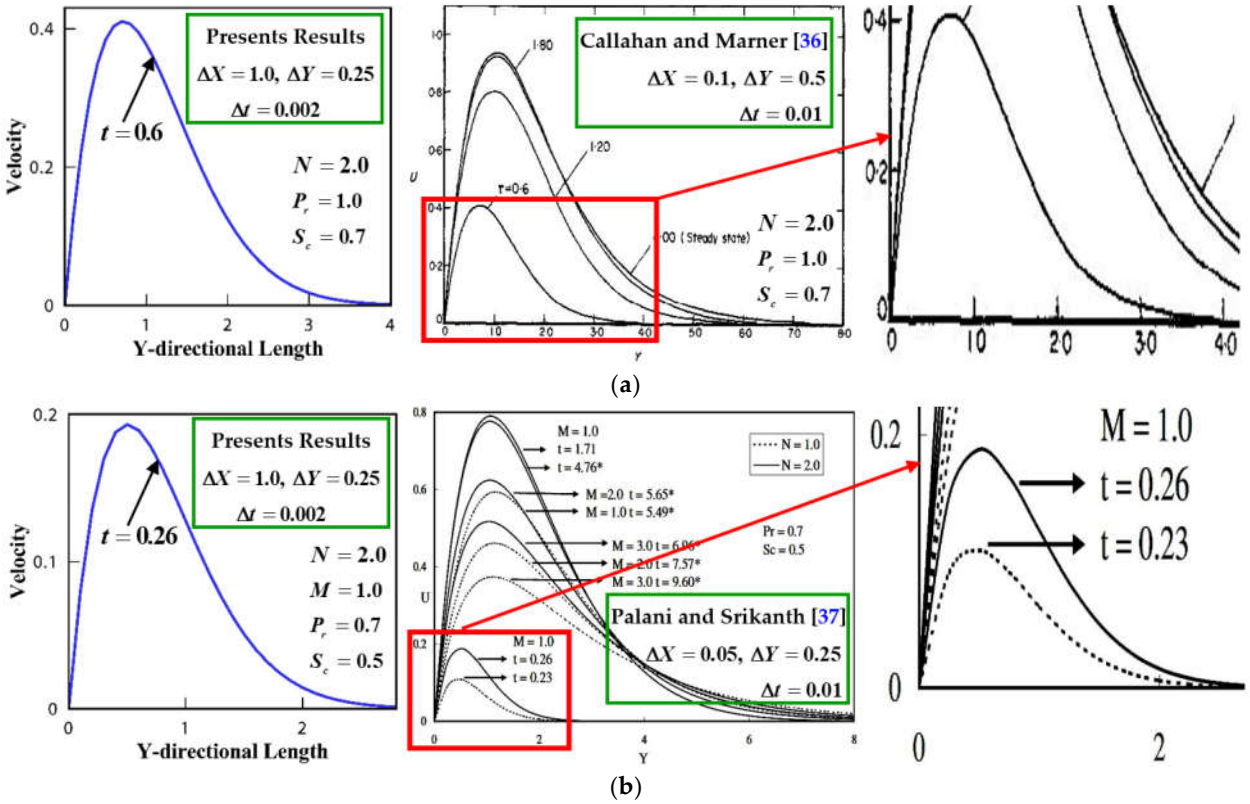

Figure 3. Graphical Comparison of fluid velocity with existing (**a**) explicit finite difference solution ([36], Figure 1, page 169) and (**b**) implicit finite difference solution ([37], Figure 3, page 352).

In order to show the effects of various parameters on flow variables, the collected numerical values have been plotted in figures by the help of data visualization software TECPLOT (American Company Tecplot, Inc., Bellevue, WA, USA). The time dependent flow variables related to the problem versus Y-directional length are illustrated in Figures 4–10.

The transient velocity distributions have been shown in Figures 4 and 5. It is found that the fluid velocities increase dramatically with time until at $t = 20$ when a steady-state value is reached. We observe from Figure 4a, for extremely cooled plate $(G_r > 0)$, the fluid velocity increases with the increase of Grashof number. The effect of the Darcy number on velocity field is presented in Figure 4b. It is observed that the velocity rapidly decreases in case of strong Darcy number. The Figure 4c shows that the fluid velocity decreases near the plate but increases far away from the plate with the increase of magnetic force number. The effect of the heat absorption parameter on velocity field is presented in Figure 5a. It is declared that the velocity decreases in case of strong heat absorption parameter. In Figure 5b, we see that the velocity decreases in case of strong Prandtl number i.e., the velocity is higher for air than water. A same effect on velocity field is noted from Figure 5c for increasing the value of Schmidt number. In particular, the velocity is larger for helium than carbon dioxide. Hence, it is concluded that the maximum velocity occurs in the vicinity of the plate.

The time dependent microrotational velocity profiles are displayed in Figures 6 and 7. It is noted that the microrotational velocities decrease significantly to a steady-state value at the time $t = 20$. We observe from Figure 6a, the microrotational velocity falls with the increase of Grashof number. The effects of Darcy number on microrotational velocity are shown in Figure 6b. We see that the microrotational velocity increases with the rise of Darcy number. A decreasing effect far away from the plate on microrotational velocity is observed from Figure 6c for increasing the spin gradient viscosity. Figure 7a declares that the microrotational velocity is decreasingly affected by Soret number. In Figure 7b, we find that the microrotational velocity slowly raises in case of strong Prandtl number. The velocity distributions in Figure 7c represent that the microrotational velocity increases with the increase of Schmidt number.

The induced magnetic field for cooling plate is displayed in Figure 8 and we see that they fall sharply with time until at $t = 20$. It is observed from Figure 8a that the induced magnetic field increases near the plate but decreases far away from plate with the increase of magnetic diffusivity number. Figure 8b shows that the induced magnetic field increases with the rise of Darcy number. A decreasing effect of magnetic force number on induced magnetic field is observed from Figure 8c.

The transient temperature distributions are shown in Figure 9. It is declared that the fluid temperature rises considerably with time until a steady-state value is obtained. The transient temperature profiles for different values of Eckert number are presented in Figure 9a and it is noticed that the increase of Eckert number leads to a rise in fluid temperature. An important effect on temperature is found from Figure 9b and we observe that temperature rapidly decreases with the increase of Prandtl number. This is due to the fact that there would be a decrease of thermal boundary layer thickness for the increase of Prandtl number. An increasing effect on temperature is observed in Figure 9c with the increase of Dufour Number.

The species concentration profiles are presented in Figure 10. It is observed that the concentration increases substantially with time until at $t = 20$. Figure 10a shows that the concentration increases in case of strong heat absorption parameter. The thermal diffusion effect is shown in Figure 10b and it is noticed that concentration gradually increases with the increase of Soret number. For different gases like helium, water vapor and carbon dioxide, concentration profiles are displayed in Figure 10c. The figure shows that a decreasing effect on concentration in case of strong Schmidt number. Physically, the increase of Schmidt number means decrease of molecular diffusivity. Hence, the concentration of species is higher for small values of the Schmidt number and lower for large values of Schmidt number. It is concluded that the maximum of concentration occurs on the plate and the thinning effect is noted for heavier particles.

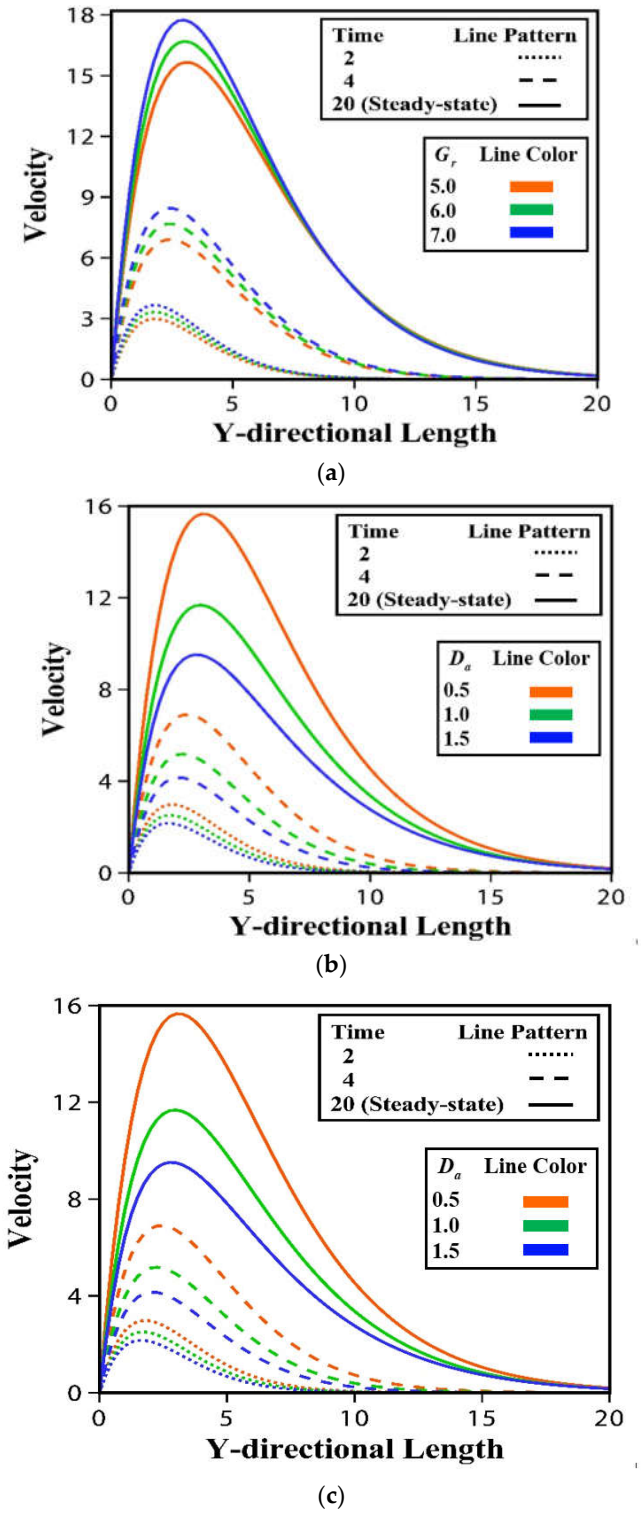

Figure 4. Velocity profiles for different values of (**a**) Grashof number (**b**) Darcy number (**c**) magnetic force number.

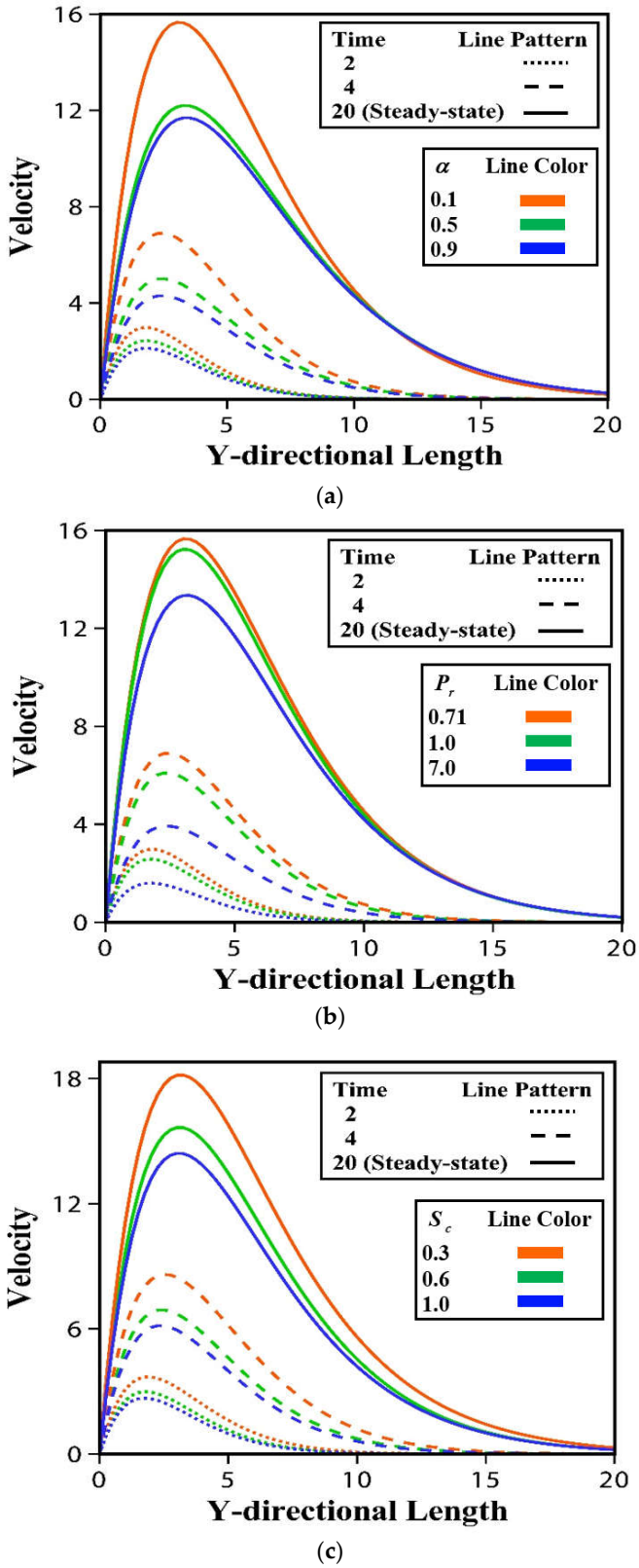

Figure 5. Velocity profiles for different values of (**a**) heat absorption parameter (**b**) Prandtl number (**c**) Schmidt number.

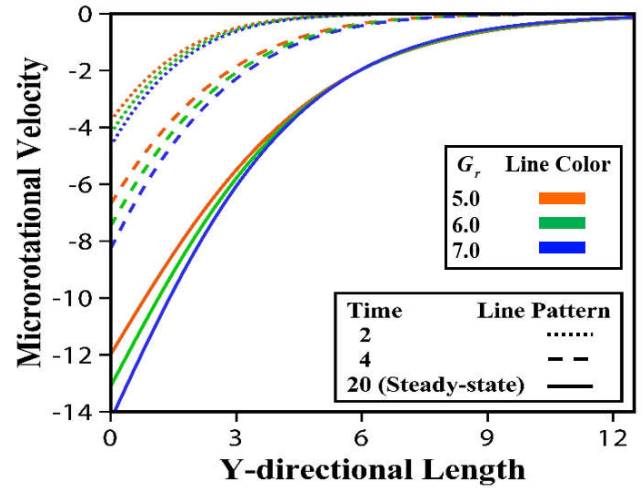

(**a**)

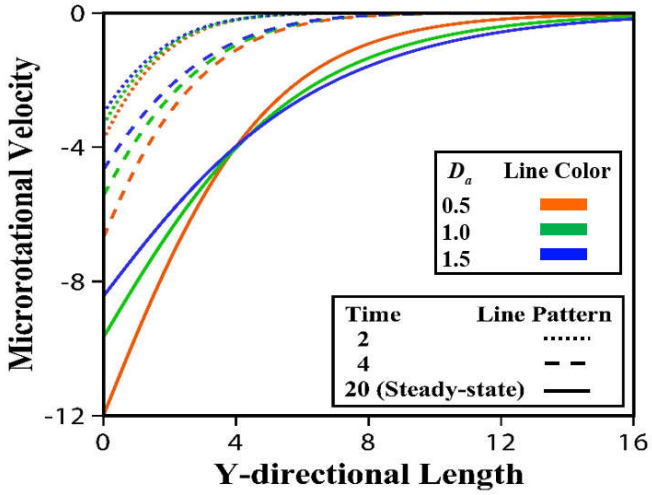

(**b**)

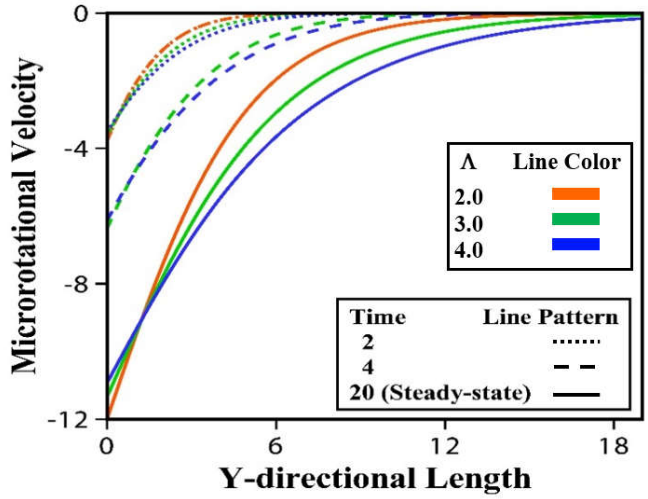

(**c**)

Figure 6. Microrotational velocity profiles for different values of (**a**) Grashof number (**b**) Darcy number (**c**) spin gradient viscosity.

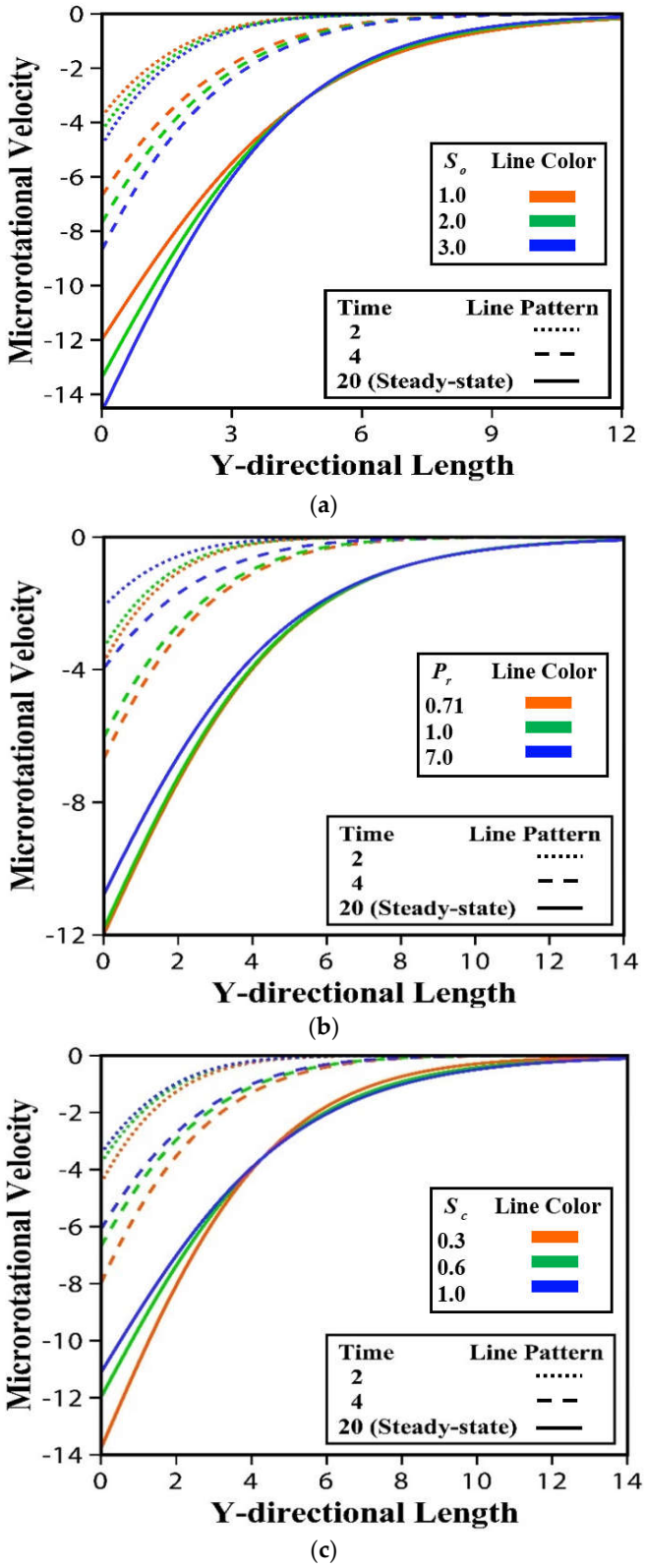

Figure 7. Microrotational velocity profiles for different values of (**a**) Soret number (**b**) Prandtl number (**c**) Schmidt number.

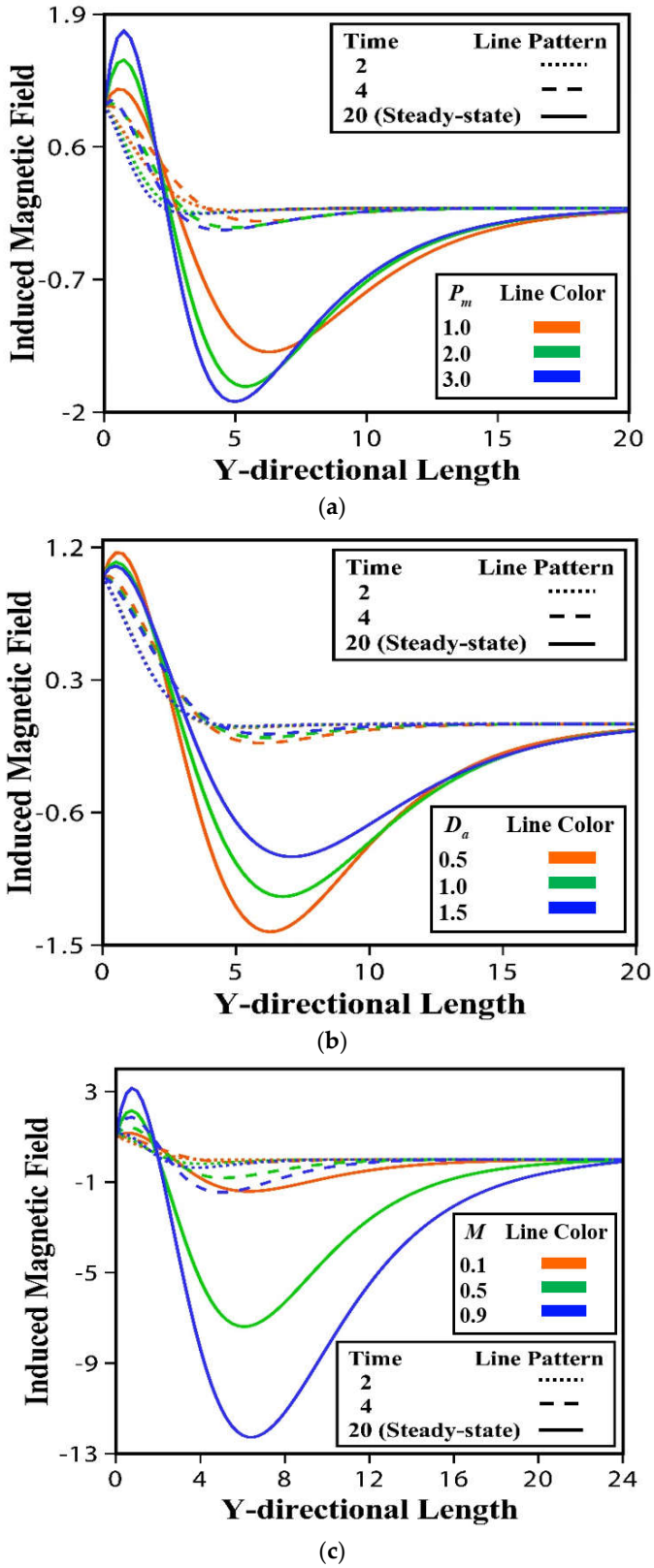

Figure 8. Induced Magnetic field profiles for different values of (**a**) magnetic diffusivity number (**b**) Darcy number (**c**) magnetic force number.

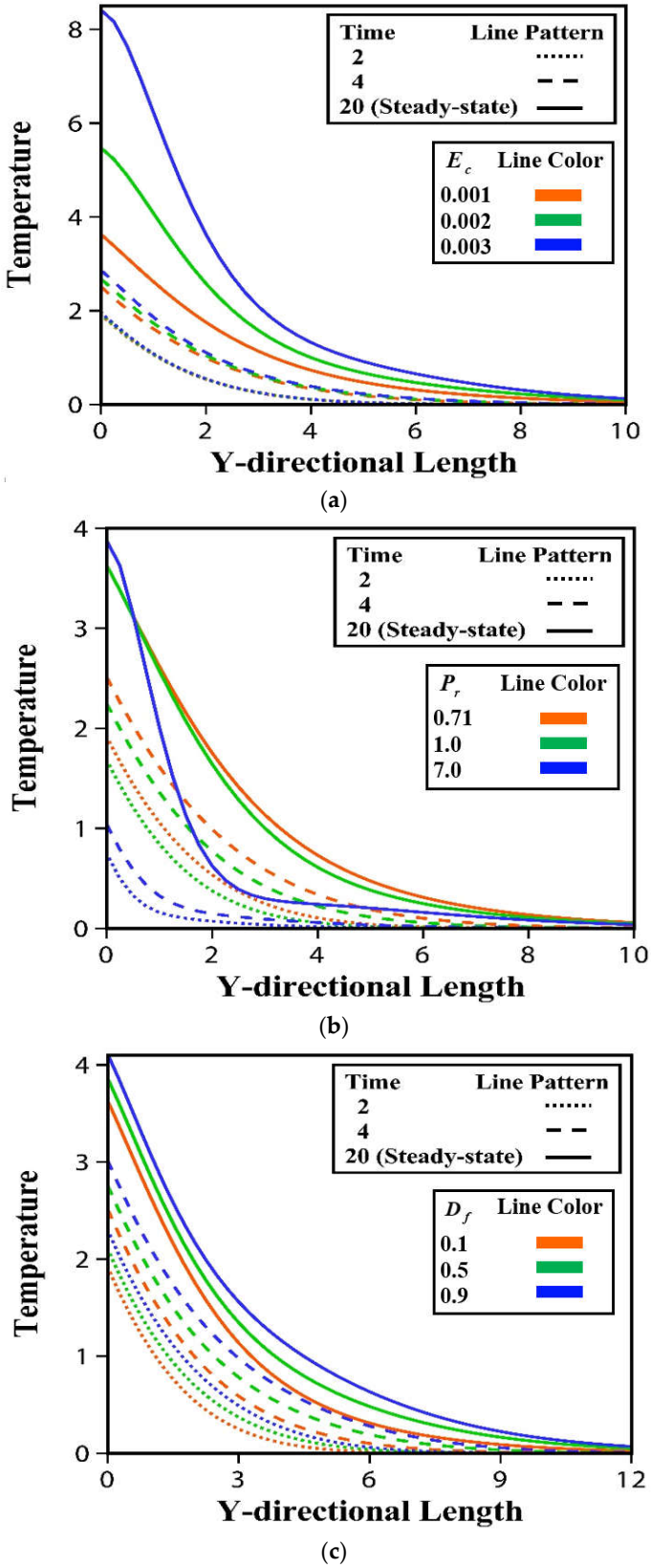

Figure 9. Temperature profiles for different values of (**a**) Eckert number (**b**) Prandtl number (**c**) Dufour number.

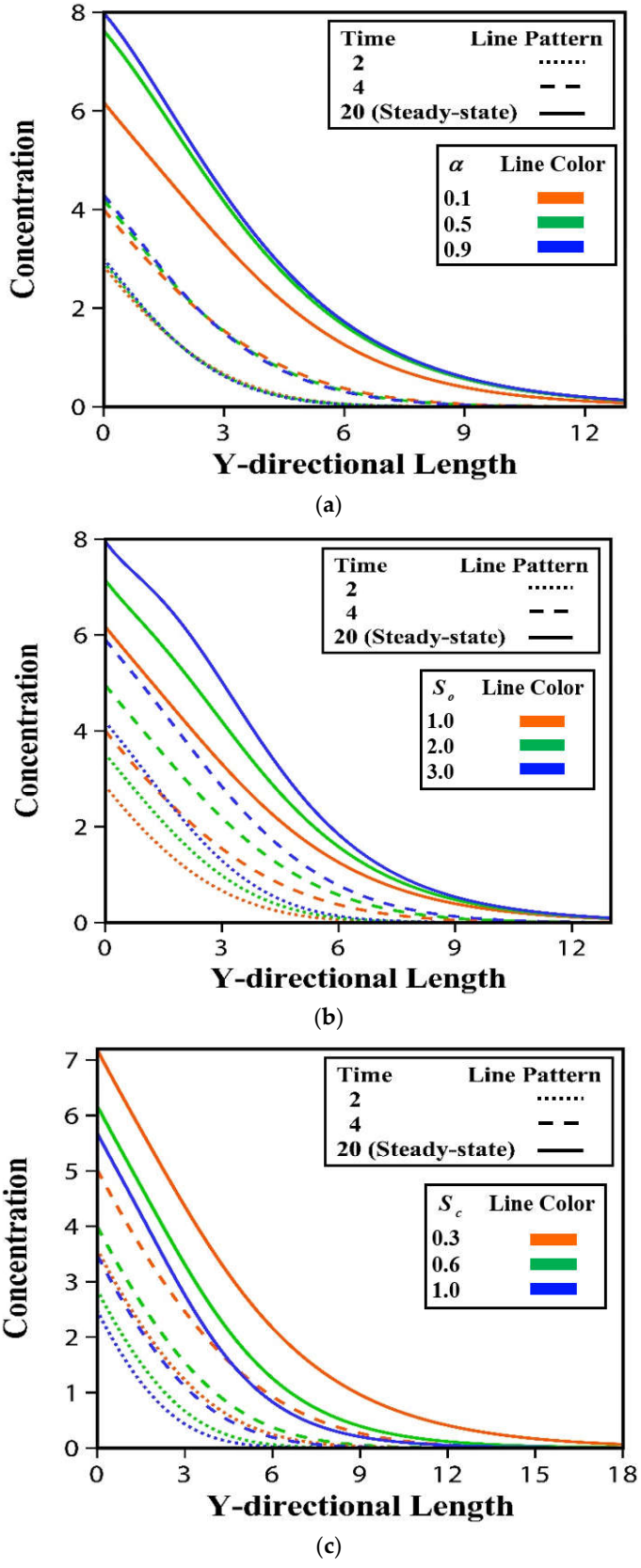

Figure 10. Concentration profiles for different values of (**a**) heat absorption parameter (**b**) Soret number (**c**) Schmidt number.

Now we attempt to discuss about the behavior of the quantities of chief physical interest of the flow. For this purpose, the solutions of shear stress, couple stress, current density, Nusselt number and Sherwood number for different values of associated parameters are computed and the obtained local and average numerical values versus *X*-directional length and time respectively are plotted in Figures 11–15.

For the different values of Grashof number, Prandtl number and Schmidt number, the curves of shear stress are drawn in Figure 11. We see that both local and average shear stress increases in case of strong Grashof number while it decreases with the increase of Prandtl number or Schmidt number. Figure 12 shows that the couple stress decreases for the increase of spin gradient viscosity, Darcy number or Schmidt number. It is observed from Figure 13 that the current density rises in case of strong Darcy number but falls with the increase of magnetic diffusivity number or magnetic force number. A decreasing effect on Nusselt number for increasing values of Dufour Number, Prandtl or Eckert number is noted from Figure 14. From the last Figure 15, we see that both local and average Sherwood number is decreasingly affected by Schmidt number or heat absorption parameter while increasingly affected by Soret number.

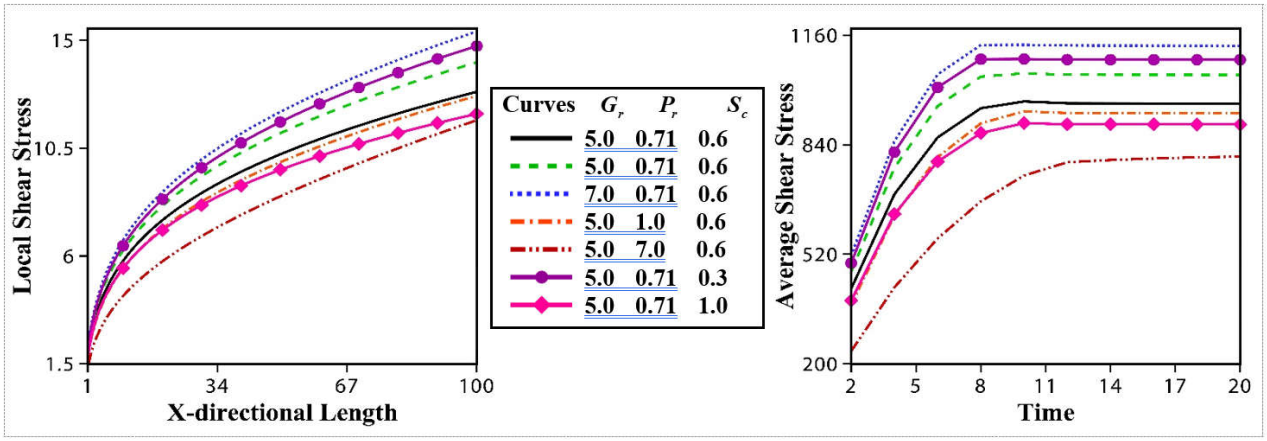

Figure 11. Effect of flow variables on local and average shear stress.

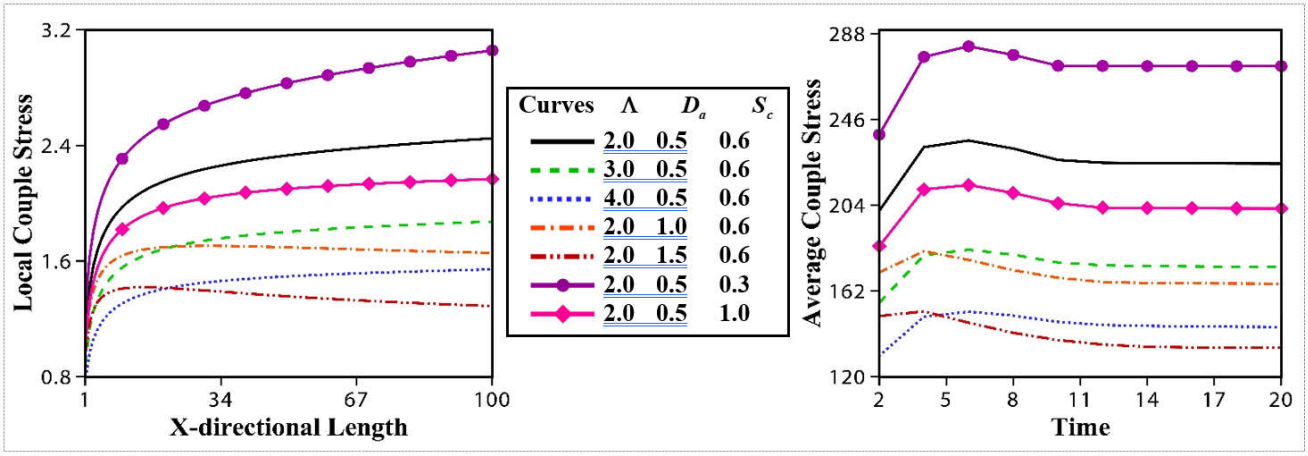

Figure 12. Effect of flow variables on local and average couple stress.

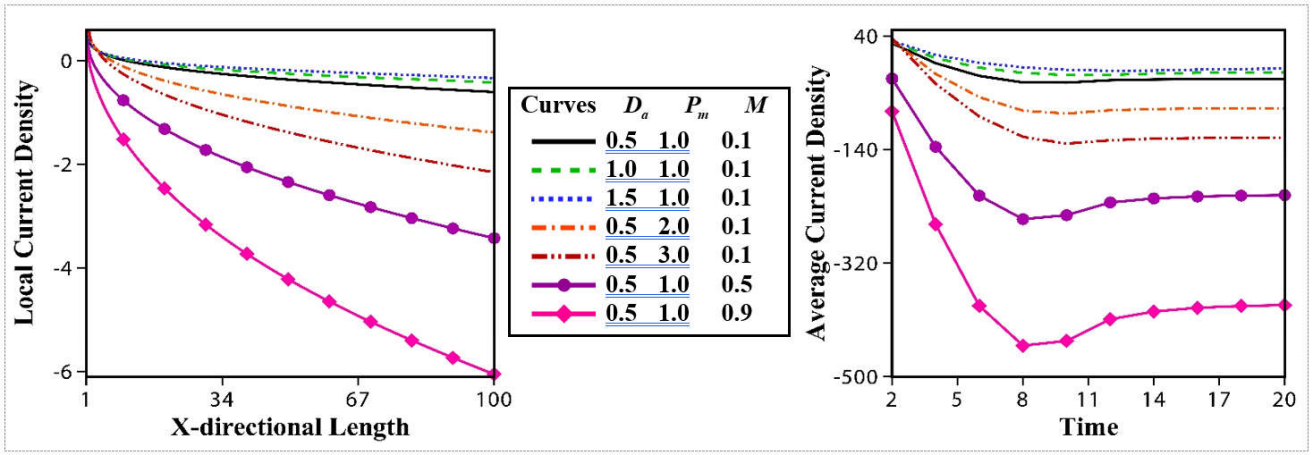

Figure 13. Effect of flow variables on local and average current density.

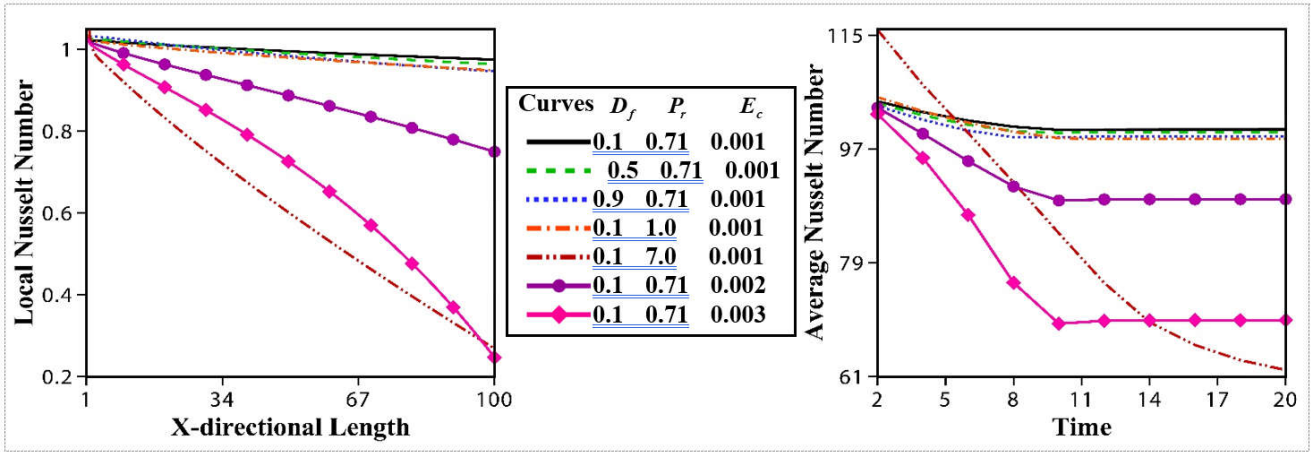

Figure 14. Effect of flow variables on local and average Nusselt number.

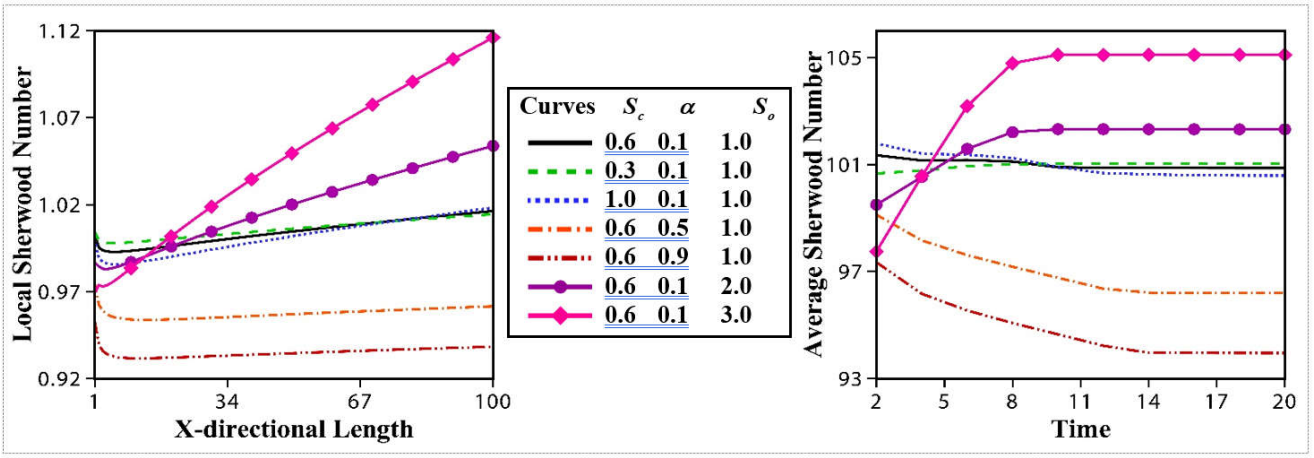

Figure 15. Effect of flow variables on local and average Sherwood number.

6. Conclusions

The induced magnetic field effect on an unsteady MHD free convective heat and mass transfer flow of a micropolar fluid past a semi-infinite vertical plate bounded by a porous medium which is subjected to constant heat and mass fluxes under the action of a strong magnetic field taking into account a constant heat sink is investigated in this work. The resulting governing system of dimensionless coupled non-linear partial differential equations are numerically solved by an explicit finite difference method. A graphical comparison between the current results and existing results of previous works is also made here. The agreement with finite difference solutions in both explicit and implicit schemes is found to be very good. Finally, the results are discussed for different values of flow parameters and the important findings that obtained from the graphical representation of the results are listed below.

i. All of the flow variables except microrotational velocity and induced magnetic field increase significantly until the steady-state value with time.
ii. Only the Grashof number enhances the fluid velocity near at the plate. It is concluded that the Grashof number plays an important role on fluid velocity in case of cooling problem.
iii. The microrotational velocity of fluid particles is positively influenced by Darcy number but negatively influenced by spin gradient viscosity.
iv. The induced magnetic field strength is stronger for the lowest magnetic force or diffusivity numbers.
v. The fluid temperature is found to be high in case of strong mass diffusion. Particularly, the fluid temperature is grater for air than water.
vi. The species concentration is increasingly affected by the both heat sink and thermal diffusion. It is also confirmed that the concentration level of fluid is greater for lighter particles than heavier particles.

It is expected that the recent study of the combined heat and mass transfer flow of micropolar fluid can be utilized in many scientific research related to the flow under induced magnetic field. The key findings may be effective in the movement of underground natural assets, in separation processes as well as in the research of geophysical fluid dynamics.

Funding: This research was funded by a Technology Invention, Research & Development (R&D) Project under the Ministry of Science and Technology (MOST), People's Republic of Bangladesh, Grant No. 39.012.002.02.01.013.2011-274-27.

Acknowledgments: The author would like to express his sincere thanks for the financial support of the Ministry of Science and Technology (MOST). The author is also grateful to the reviewers for their valuable suggestions and constructive comments.

Conflicts of Interest: The author declares no conflict of interest.

Nomenclature

$\overline{C}$	species concentration
C	dimensionless species concentration
c_s	concentration susceptibility
c_p	specific heat at constant pressure
C_∞	species concentration of uniform flow
D_a	Darcy number
D_m	coefficient of mass diffusivity
D_f	Dufour number
E_c	Eckert number
g	local acceleration due to gravity
G	microrotation vector

G_r	Grashof number
G_m	modified Grashof number
h_s	constant heat sink
$\mathbf{H}$	induced magnetic field vector
H	dimensionless induced magnetic field component
H_0	induced magnetic field strength
H_w	induced magnetic field at the wall
H_x, H_y	induced magnetic field components
j	microinertia per unit mass
K	permeability of the medium
m	constant mass flux per unit area
M	magnetic force number
P_m	magnetic diffusivity number
P_r	Prandtl number
Q	constant heat flux per unit area
S	microrotational constant
S_c	Schmidt number
S_o	Soret number
t	dimensionless time
$\bar{T}$	fluid temperature
T	dimensionless fluid temperature
T_m	mean fluid temperature
T_∞	fluid temperature of uniform flow
u, v	velocity components
U, V	dimensionless velocity components
U_0	dimensionless constant velocity
x	spatial coordinate along to the plate
X	dimensionless spatial coordinate along to the plate
y	spatial coordinate normal to the plate
Y	dimensionless spatial coordinate normal to the plate

Greek Symbols

∇	divergence vector
Δ	microrotational number
Δt	dimensionless time-step
ΔX	dimensionless mesh sizes along X direction
ΔY	dimensionless mesh sizes along Y direction
Λ	spin gradient viscosity
α	heat absorption parameter
β	thermal expansion coefficient
β^*	concentration expansion coefficient
χ	vortex viscosity
γ	spin-gradient viscosity
κ	thermal conductivity
κ_T	thermal diffusion ratio
λ	vortex viscosity
μ_e	magnetic permeability
ρ	density of the fluid
σ	electrical conductivity
τ	time
Γ	dimensionless microrotational component
$\bar{\Gamma}$	microrotational component
υ	kinematic viscosity

Subscripts

W	at the wall of the plate
∞	free stream conditions
i, j	grid points along x and y axis respectively
Superscript	
n	number of time-steps
$'$	at the end of a time-step

References

1. Eringen, A.C. Theory of micropolar fluids. *J. Math. Mech.* **1966**, *16*, 1–18.
2. Eringen, A.C. Theory of thermomicrofluids. *J. Math. Anal. Appl.* **1972**, *38*, 480–496.
3. Jena, S.K.; Mathur, M.N. Similarity solutions for laminar free convection flow of a thermomicropolar fluid past a non-isothermal vertical flat plate. *Int. J. Eng. Sci.* **1981**, *19*, 1431–1439.
4. Gorla, R.S.R.; Takhar, H.S.; Slaouti, A. Magnetohydrodynamic free convection boundary layer flow of a thermomicropolar fluid over a vertical plate. *Int. J. Eng. Sci.* **1998**, *36*, 315–327.
5. El-Amin, M.F. Magnetohydrodynamic free convection and mass transfer flow in micropolar fluid with constant suction. *J. Magn. Magn. Mater.* **2001**, *234*, 567–574.
6. Haque, M.M.; Alam, M.M.; Ferdows, M.; Postelnicu, A. MHD free convective heat generating unsteady micropolar fluid flow through a porous medium with constant heat and mass fluxes. *Eur. J. Sci. Res.* **2011**, *53*, 491–515.
7. Bhattacharyya, K.; Mukhopadhyay, S.; Layek, G.C.; Pop, I. Effects of thermal radiation on micropolar fluid flow and heat transfer over a porous shrinking sheet. *Int. J. Heat Mass Transf.* **2012**, *55*, 2945–2952.
8. Safaei, M.R.; Ahmadi, G.; Goodarzi, M.S.; Kamyar, A.; Kazi, S.N. Boundary layer flow and heat transfer of FMWCNT/water nanofluids over a flat plate. *Fluids* **2016**, *1*, 31.
9. Waqas, M.; Farooq, M.; Khan, M.I.; Alsaedi, A.; Hayat, T.; Yasmeen, T. Magnetohydrodynamic (MHD) mixed convection flow of micropolar liquid due to nonlinear stretched sheet with convective condition. *Int. J. Heat Mass Transf.* **2016**, *102*, 766–772.
10. Turkyilmazoglu, M. Flow of a micropolar fluid due to a porous stretching sheet and heat transfer. *Int. J. Non-Linear Mech.* **2016**, *83*, 59–64.
11. Mahabaleshwar, U.S.; Sarris, I.E.; Lorenzini, G. Effect of radiation and Navier slip boundary of Walters' liquid B flow over a stretching sheet in a porous media. *Int. J. Heat Mass Transf.* **2018**, *127*, 1327–1337.
12. Benos, L.T.; Mahabaleshwar, U.S.; Sakanaka, P.H.; Sarris, I.E. Thermal analysis of the unsteady sheet stretching subject to slip and magnetohydrodynamic effects. *Therm. Sci. Eng. Prog.* **2019**, *13*, 100367.
13. Abdal, S.; Ali, B.; Younas, S.; Ali, L.; Mariam, A. Thermo-diffusion and multislip effects on MHD mixed convection unsteady flow of micropolar nanofluid over a shrinking/stretching sheet with radiation in the presence of heat source. *Symmetry* **2020**, *12*, 49.
14. Jamaludin, A.; Naganthran, K.; Nazar, R.; Pop, I. MHD mixed convection stagnation-point flow of Cu-Al2O3/water hybrid nanofluid over a permeable stretching/shrinking surface with heat source/sink. *Eur. J. Mech. B Fluids* **2020**, *84*, 71–80.
15. Murtaza, M.G.; Tzirtzilakis, E.E.; Ferdows, M. Stability and convergence analysis of a biomagnetic fluid flow over a stretching sheet in the presence of a magnetic field. *Symmetry* **2020**, *12*, 253.
16. Gaffar, S.A.; Bég, O.A.; Prasad, V.R. Mathematical modeling of natural convection in a third-grade viscoelastic micropolar fluid from an isothermal inverted cone. *Iran. J. Sci. Technol. Trans. Mech. Eng.* **2020**, *44*, 383–402.
17. Bidin, B.; Rees, D.A.S. The onset of convection in an unsteady thermal boundary layer in a porous medium. *Fluids* **2016**, *1*, 41.
18. Vasu, B.; Gorla, R.S.R.; Murthy, P.V.S.N.; Prasad, V.R.; Bég, O.A.; Siddiqa, S. MHD free convection-radiation interaction in a porous medium-Part II: Soret/Dufour effects. *Int. J. Appl. Mech. Eng.* **2020**, *25*, 157–175.
19. Gupta, Y.; Rana, P.; Bég, O.A.; Kadir, A. Multiple solutions for slip effects on dissipative magneto-nanofluid transport phenomena in porous media: Stability analysis. *J. Appl. Comput. Mech.* **2020**, *6*, 956–967.
20. Khashi'ie, N.S.; Arifin, N.M.; Pop, I. Non-Darcy mixed convection of hybrid nanofluid with thermal dispersion along a vertical plate embedded in a porous medium. *Int. Commun. Heat Mass Transf.* **2020**, *118*, 104866.
21. Benos, L.T.; Polychronopoulos, N.D.; Mahabaleshwar, U.S.; Lorenzini, G.; Sarris, I.E. Thermal and flow investigation of MHD natural convection in a nanofluid-saturated porous enclosure: An asymptotic analysis. *J. Therm. Anal. Calorim.* **2021**, *143*, 751–765.
22. Karvelas, E.; Sofiadis, G.; Papathanasiou, T.; Sarris, I. Effect of micropolar fluid properties on the blood flow in a human carotid model. *Fluids* **2020**, *5*, 125.
23. Chaudhary, R.C.; Sharma, B.K. Combined heat and mass transfer by laminar mixed convection flow from a vertical surface with induced magnetic field. *J. Appl. Phys.* **2006**, *99*, 034901.
24. Alam, M.M.; Islam, M.R.; Rahman, F. Steady heat and mass transfer by mixed convection flow from a vertical porous plate with induced magnetic field, constant heat and mass fluxes. *Thammasat Int. J. Sci. Technol.* **2008**, *13*, 1–13.
25. Haque, M.M.; Alam, M.M. Transient heat and mass transfer by mixed convection flow from a vertical porous plate with induced magnetic field, constant heat and mass fluxes. *Model. Meas. Control B* **2009**, *78*, 54–73.

26. Sultana, M.; Haque, M.M.; Alam, M.M.; Ferdows, M.; Postelnicu, A. Micropolar fluid behavior on MHD heat transfer flow through a porous medium with induced magnetic field by finite difference method. *Eur. J. Sci. Res.* **2011**, *53*, 477–490.
27. Haque, M.M.; Alam, M.M.; Ferdows, M.; Al-Mdallal, Q.M. Numerical simulation and stability analysis on MHD free convective heat and mass transfer unsteady flow through a porous medium in a rotating system with induced magnetic field. *Int. J. Appl. Electromagn. Mech.* **2013**, *41*, 121–141.
28. Ibrahim, W. The effect of induced magnetic field and convective boundary condition on MHD stagnation point flow and heat transfer of nanofluid past a stretching sheet. *IEEE Trans. Nanotechnol.* **2015**, *14*, 178–186.
29. Hossain, K.E.; Haque, M.M. Influence of magnetic field on chemically reactive blood flow through stenosed bifurcated arteries. *Aip Conf. Proc.* **2017**, *1851*, 020012.
30. Aslani, K.-E.; Benos, L.; Tzirtzilakis, E.; Sarris, I.E. Micromagnetorotation of MHD micropolar flows. *Symmetry* **2020**, *12*, 148.
31. Haque, M.M.; Ferdows, M.; Alam, M.M. Explicit finite difference and steady-state solutions of heat and mass transfer flow from a vertical porous plate with thermal diffusion and induced magnetic field. *Acta Tech. CSAV* **2017**, *62*, 13–26.
32. Islam, M.M.; Haque, M.M. Radiative Walter's memory flow along a vertical cone in induced magnetic field with thermophoretic effect. *Aip Conf. Proc.* **2017**, *1851*, 020015.
33. Akmal, N.; Sagheer, M.; Hussain, S.; Kamran, A. Investigation of free convection in micropolar nanofluid with induced magnetic field. *Eur. Phys. J. Plus* **2019**, *134*, 235.
34. Baruah, I.; Hazarika, G.C. Behaviour of Soret and Dufour effects on unsteady micropolar fluid considering viscosity and thermal conductivity as variable quantities under mixed convection and mass transfer. *Int. J. Math. Trends Technol.* **2018**, *58*, 231–239.
35. Singh, K.; Kumar, M. Melting and heat absorption effects in boundary layer stagnation-point flow towards a stretching sheet in a micropolar fluid. *Ain Shams Eng. J.* **2018**, *9*, 861–868.
36. Callahan, G.D.; Marner, W.J. Transient free convection with mass transfer on an isothermal vertical flat plate. *Int. J. Heat Mass Transf.* **1976**, *19*, 165–174.
37. Palani, G.; Srikanth, U. MHD flow past a semi-infinite vertical plate with mass transfer. *Nonlinear Anal. Model. Control* **2009**, *14*, 345–356.